

Disorder controlled sound speed and thermal conductivity of hybrid metalcone films

Md Shafkat Bin Hoque, Rachel A. Nye, Saman Zare, Stephanie Atkinson, Siyao Wang, Andrew H. Jones, John T. Gaskins, Gregory Parsons, and Patrick E. Hopkins

Md Shafkat Bin Hoque, Saman Zare

Department of Mechanical and Aerospace Engineering, University of Virginia, Charlottesville, Virginia 22904, USA

Rachel A. Nye, Stephanie Atkinson, Siyao Wang, Gregory Parsons

Department of Chemical and Biomolecular Engineering, North Carolina State University, Raleigh, North Carolina 27606, United States

Andrew H. Jones, John T. Gaskins

Laser thermal Inc., Charlottesville, Virginia 22902, USA

Patrick E. Hopkins

Department of Mechanical and Aerospace Engineering, University of Virginia, Charlottesville, Virginia 22904, USA

Department of Materials Science and Engineering, University of Virginia, Charlottesville, Virginia 22904, USA

Department of Physics, University of Virginia, Charlottesville, Virginia 22904, USA

Email: phopkins@virginia.edu

arXiv:2402.13215v1 [physics.app-ph] 20 Feb 2024

Abstract

The multifaceted applications of polymers are often limited by their thermal conductivity. Therefore, understanding the mechanisms of thermal transport in polymers is of vital interest. Here, we leverage molecular layer deposition to grow three types of hybrid metalcone (i.e., alucone, zincone, and tincone) films and study their thermal and acoustic properties. The thermal conductivity of the hybrid polymer films ranges from 0.43 to 1.14 W m⁻¹ K⁻¹. Using kinetic theory, we trace the origin of thermal conductivity difference to sound speed change, which is dictated by the structural disorder within the films. Changing the disorder has negligible impacts on volumetric heat capacity and vibrational lifetimes. Our findings provide means to improve the thermal conductivity of organic, hybrid, and inorganic polymer films.

Keywords: *Molecular layer deposition, thermal conductivity, vibrational lifetime, metalcone*

1 Introduction

The thermal, acoustic, and optical properties of polymers have been widely studied in literature due to their applications in electronic devices as flexible substrates, encapsulation layers, and insulating materials.¹⁻⁶ The thermal conductivity of polymers can span across three orders of magnitude; ranging from 0.2 W m⁻¹ K⁻¹ in PMMA⁷ to 23 W m⁻¹ K⁻¹ in Zylon HM.⁸ Structural disorder and type of interactions between the polymer chains generally control the thermal conductivity of polymers.⁹⁻¹³ However, establishing a clear physical picture of thermal transport in polymers has been a challenge. Study of new types of polymers with different degree of structural disorder can shed light onto this aspect.

Only recently, molecular layer deposition (MLD)⁵ has been successful in growing different types of stable hybrid organic-inorganic metalcone polymers. MLD uses a bifunctional organic monomer and multifunctional inorganic precursor to grow the hybrid metalcone films.¹⁴ In addition to the usual applications of polymers, hybrid polymers are also useful in organic light emitting diodes and lithium/sodium ion batteries.¹⁵⁻¹⁷ Use of metalcone films in these devices has resulted in improved lifetimes and stability. However, due to the relatively new age of the metalcone films, their thermal and acoustic properties remain unexplored.

In this study, we characterize the thermal and acoustic properties of three different types of metalcone films—alucone, zincone, and tincone—grown via MLD. The three metalcone films each possess a different degree of structural disorder (characterized by double reactions) based on growth. We use steady-state thermorefectance (SSTR)¹⁸⁻²⁰ and time-domain thermorefectance (TDTR)²¹⁻²³ to measure the thermal conductivity and longitudinal sound speed of the films, respectively. Our measurements reveal that the structural disorder controls the longitudinal sound speed of the films. The sound speed, in turn, dictates the thermal conductivity of the metalcone films. We further verify the findings by measuring thermal conductivity, longitudinal sound speed, volumetric heat capacity, and lifetime of the vibration modes of an ordered and disordered alucone film. Our study opens up new pathways for tuning the thermal and acoustic properties of hybrid polymer films by manipulating disorder.

2 Growth details of the metalcone films

The metalcone films are deposited via MLD using various metalorganic precursors and ethylene glycol (EG) as the coreactants. Alucone is deposited from trimethylaluminum (TMA) and EG. Zincone is deposited from diethyl zinc (DEZ) and EG.²⁴ Tincone is deposited from tetrakis (dimethylamido)

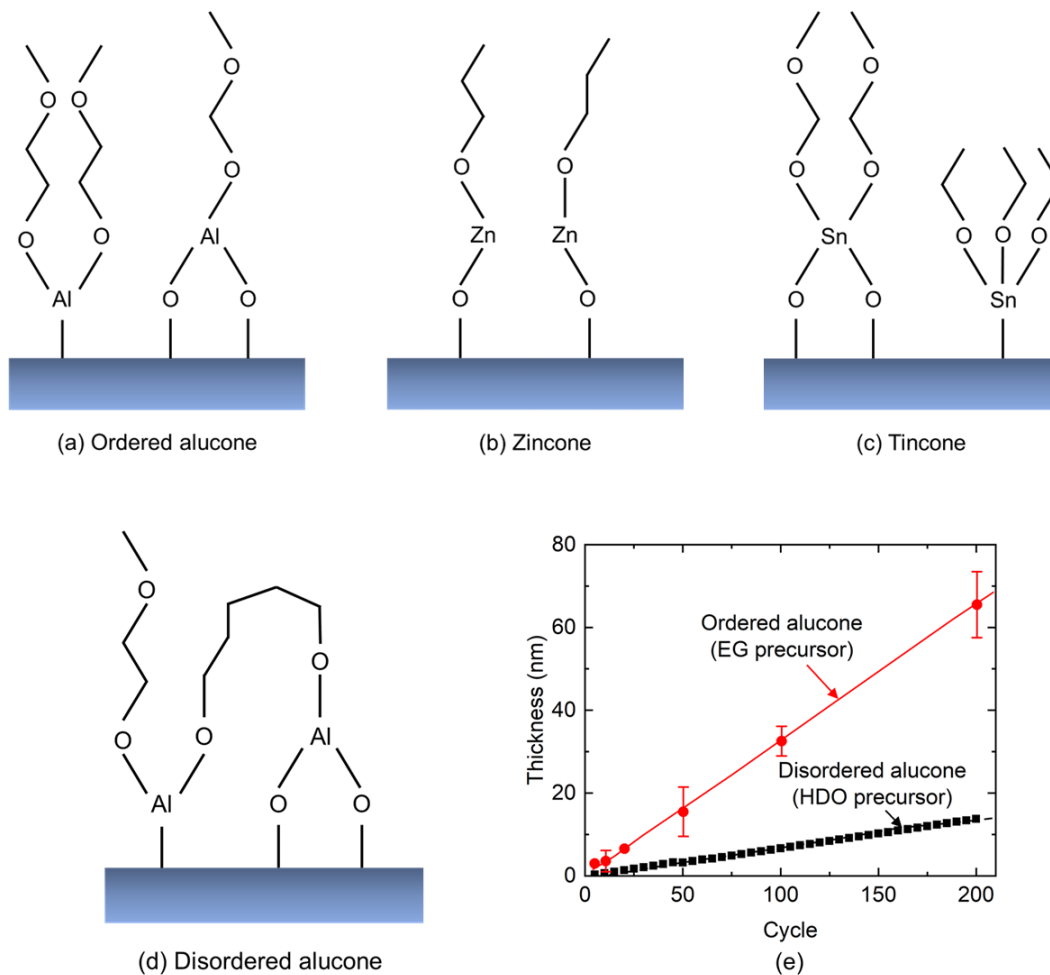


Figure 1: Structures of the (a) ordered alucone, (b) zincone, (c) tincone, and (d) disordered alucone films. (e) Growth rate of the ordered and disordered alucone films measured by ellipsometry.

tin (TDMASn) and EG. Each precursor is handled only in nitrogen-ambient before being installed on the home-built cylindrical or spherical MLD reactors.^{5,25} Precursors are heated as follows to achieve sufficient vapor pressure for deposition: TDMASn to 65 °C, TMA to room temperature, DEZ to room temperature, and EG to 80 °C for alucone and 70 °C for tincone and zincone. The deposition is carried out at 100 °C and 400 mTorr. The silicon (Si) substrates are cleaned in a piranha solution of 1:1 volume ratio H₂O₂:H₂SO₄ for 15 minutes before use. The structures of the metalcone films are shown in Figure 1. The thicknesses of the films range from 1 to 156 nm.

To study the effects of disorder on the thermal and acoustic properties of the metalcone films, we also deposit alucone films from TMA and 1,6-hexamethylenediol (HDO). While alucone films from

TMA/EG is common, HDO represents a more unique and much less studied reactant. The alucone film grown from HDO precursors are less ordered compared to that of EG as discussed in the next section. As a result, we define the HDO alucone films as disordered in this study.

3 Characterization of structural disorders in the films

We characterize the disorders in the metalcone films by the phenomenon of double reactions (DRs).^{25,26} When DRs occur, both reactive groups of the homobifunctional precursors react with the growth surface during the same half-cycle without providing a new site for continued growth. DRs are more common for more flexible molecules (i.e., with longer aliphatic hydrocarbon chains). Among the metalcone films, tincone is expected to undergo a larger number of DRs during deposition compared to alucone because the tin precursor can bond with more organic ligands (4 and 3 for tincone and alucone, respectively). Increased DRs will lead to increased interactions between adjacent molecules/chains in a film, thereby increasing disorder in tincone compared to the alucone films.

Moreover, for the alucone films, the DRs are expected to be different based on the precursors (i.e., EG and HDO) used. EG is relatively short, and is expected to have few DRs and give rise to a relatively more ordered alucone film. On the other hand, the longer chain HDO precursor is expected to undergo more frequent DRs, thus resulting in more cross-linked or tangled chains during deposition and a more disordered film. The structure of a disordered alucone film is shown in Figure 1(d).

Figure 1(e) plots film thickness as a function of atomic layer deposition cycle for both alucone films (TMA/EG and TMA/HDO), as measured by spectroscopic ellipsometry. The growth rates correspond to 0.3 and 0.07 nm/cycle for alucone deposited using EG and HDO, respectively, consistent with previous results.²⁷ The higher growth rate for the less flexible precursor (i.e. EG compared to HDO) is consistent with fewer expected double reactions for EG, as observed in many MLD processes.^{5,26,28}

4 Results and discussions

The thermal and acoustic properties of the metalcone films are characterized by laser-optical thermoreflectance techniques SSTR and TDTR, respectively. We use $1/e^2$ pump and probe diameters of $\sim 20 \mu\text{m}$ for SSTR, whereas for TDTR, the diameters are ~ 20 and $11 \mu\text{m}$, respectively. Additional details of the techniques can be found in previous publications.^{18-20,23,30} To convert the optical energy of the lasers into thermal energy, we deposit a thin aluminum film atop the samples via electron beam evaporation prior to the thermoreflectance measurements.³¹

Figure 2(a) shows a schematic diagram of the sample geometry. As most of the metalcone films have thicknesses less than 50 nm, measuring thermal conductivity directly can be challenging. Therefore, we measure the total thermal resistance (R) across the entire sample geometry via SSTR. The total thermal resistance can be expressed via the following series resistor model:³¹

$$R = \left(\frac{1}{G}\right)_{Al/film} + \left(\frac{L}{\kappa}\right)_{film} + \left(\frac{1}{G}\right)_{film/Si} \quad (1)$$

Where G , κ , and L represent thermal boundary conductance, thermal conductivity, and thickness of

the metalcone films, respectively. Figure 2(b) shows the measured thermal resistances of the films as a function of thickness. As exhibited here, thermal resistance linearly increases with film thickness. For such cases, thermal conductivity can be extracted from a linear fit to the thermal resistance as a function of film thickness. Here, the inverse of the slope $(\Delta R/\Delta L)^{-1}$ provides the thermal conductivity of the films.³² Using this methodology, we determine the thermal conductivity of the metalcone films as tabulated in Table 1.

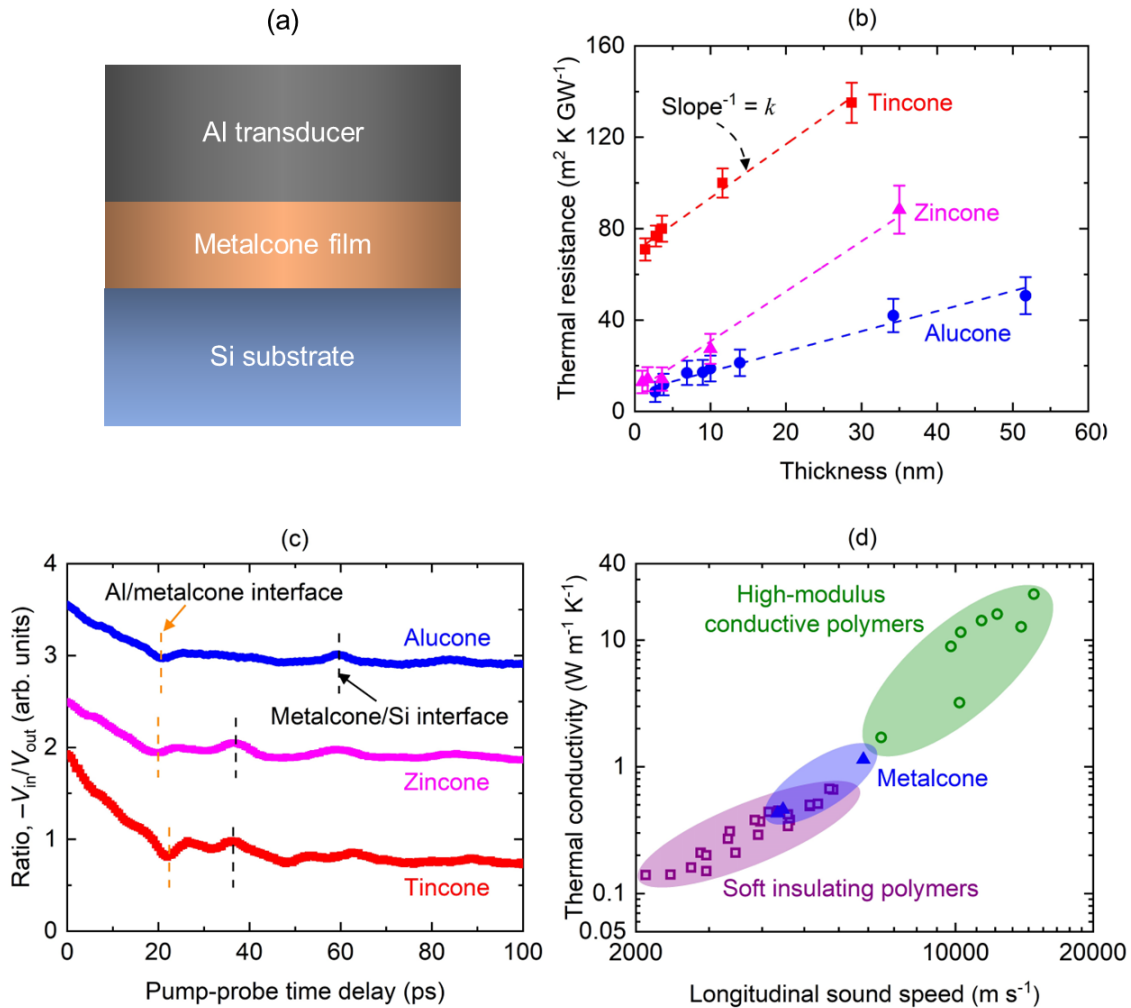


Figure 2: (a) Schematic diagram of the sample geometry. (b) Thermal resistance as a function of alucone (EG precursor), zincone, and tincone film thickness. (c) Picosecond acoustic response of TDTR measurements for a 120, 35, and 29 nm alucone (EG precursor), zincone, and tincone film, respectively. (d) Thermal conductivity vs longitudinal sound speed for a wide range of polymers. The data for the soft insulating polymers and high-modulus conductive polymers (hollow symbols) are taken from Refs^{7,8,29}.

Table 1: Thermal conductivity and longitudinal sound speed of the metalcone films.

Metalcone films	Thermal conductivity (W m ⁻¹ K ⁻¹)	Longitudinal sound speed (m s ⁻¹)
Alucone (EG precursor)	1.14 ± 0.18	6288 ± 324
Zincone	0.46 ± 0.06	4192 ± 401
Tincone	0.43 ± 0.07	4080 ± 297

We measure the longitudinal sound speed of the metalcone films via picosecond acoustics^{30,33–37} using TDTR. Figure 2(c) shows the picosecond acoustic response of the metalcone films. As exhibited in Table 1, alucone films (EG precursor) have the highest sound speed, whereas tincone films have the lowest. We posit that the sound speed difference between the two metalcone films is stemming from the difference in disorders. As sound speed is an indicator of stiffness or elastic modulus of a material,³⁴ the disorder is also changing the stiffness of the metalcone films.

According to the kinetic theory, $\kappa = \frac{1}{3}Cv^2\tau$, where C , v , and τ represent volumetric heat capacity, sound speed, and lifetime of the vibrational modes, respectively.³³ Using this equation, the thermal conductivity difference among the metalcone films can be quantitatively explained by the difference in sound speed. This provides evidence that instead of volumetric heat capacity or lifetimes, sound speed is dictating the thermal conductivity of the metalcone films. A similar trend has been observed in literature^{7,8,29} for other polymers as illustrated in Figure 2(d). This figure also shows that the metalcone films can bridge an important gap between the soft, insulating polymers and high-modulus, conductive polymers.

To further show the impact of disorders on the sound speed and thermal conductivity of the metalcone films, we measure κ , C , v , and τ of an ordered (EG precursor) and disordered (HDO precursor) alucone film. The TDTR multifrequency approach^{38,39} is used to simultaneously measure the thermal conductivity and volumetric heat capacity of 120 nm ordered and 156 nm disordered alucone films. As shown in Figure 3(a), the volumetric heat capacity remains the same for both cases: 2.0 ± 0.3 MJ m⁻³ K⁻¹. The thermal conductivity, on the other hand, drops from 1.05 ± 0.15 W m⁻¹ K⁻¹ for the ordered film to 0.5 ± 0.08 W m⁻¹ K⁻¹ for the disordered film. The longitudinal sound speed also changes from 6288 ± 324 m s⁻¹ for the ordered film to 4532 ± 230 m s⁻¹ for the disordered film. The picosecond acoustic response of the disordered alucone film is shown in Supporting Figure S1. The different thicknesses of the ordered and disordered alucone films are not expected to have an impact on the thermal conductivity and sound speed measurements.^{5,35}

The lifetimes associated with each vibrational mode in the alucone films are found from fitted oscillator models on ellipsometric data collected using IR-VASE (IR-VASE Mark II, J.A. Woollam Company). The ellipsometric data are acquired in the spectral range of 666-5000 cm⁻¹ (2-16 μ m) with a resolution of 8 cm⁻¹. The raw ellipsometric data (Ψ and Δ) are processed using multiple Gaussian oscillators to determine the dielectric function of the alucone film. The parameters of each Gaussian oscillator, including amplitude, energy centroid, and broadening, are optimized to fit the model to the collected ellipsometric data (see Supporting Information). Figure 3(b) shows the imaginary component of the dielectric function as a function of wavelength for ordered and disordered alucone films. The optical lifetimes for the identified modes are determined by taking the reciprocal of the broadening parameter associated with each Gaussian oscillator. In Figure 3(c), we plot the derived lifetime of the vibrational modes for the two cases. As exhibited here, the lifetimes are nearly identical for ordered and disordered films at all wavelengths with one exception at 8.2 μ m. The weighted average of lifetimes for the ordered film is 41

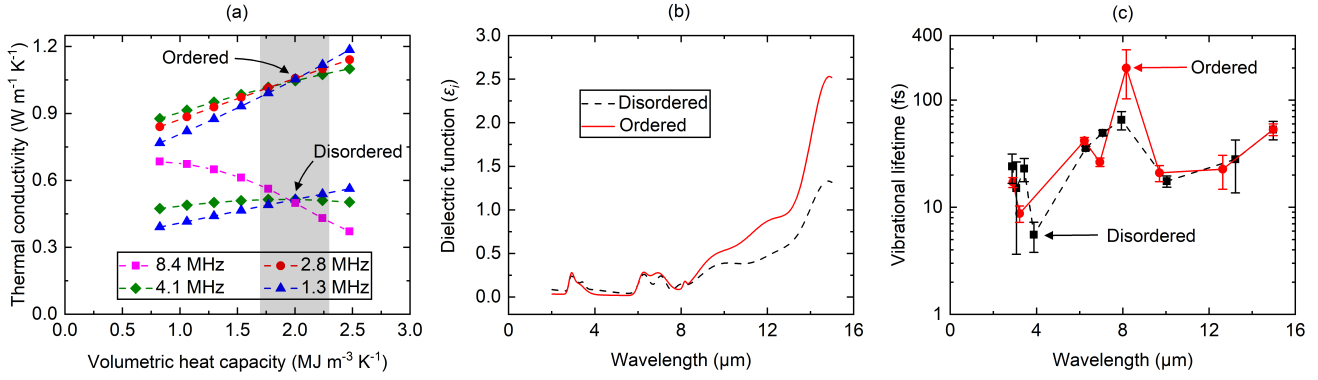


Figure 3: (a) Thermal conductivity and volumetric heat capacity of the ordered and disordered alucone film. (b) Imaginary component of the dielectric function for the two cases as a function of wavelength. (c) Lifetime of the vibrational modes in alucone films. The uncertainty associated with the lifetime measurements are $\sim 10\%$.

± 4 fs, whereas for the disordered film, it is 38 ± 5 fs. This conclusively shows that the thermal conductivity difference between the two films originates from the sound speed difference, not volumetric heat capacity or lifetimes. Our results thus provide a clear picture of thermal transport in hybrid metalcone films. The thermal and acoustic properties reported here can be useful when incorporating metalcone films in electronic, photonic, and optoelectronic devices.

5 Conclusion

In summary, we investigate the thermal and acoustic properties of alucone, zincone, and tincone films grown via MLD. Alucone possesses the highest thermal conductivity, while tincone the lowest. Structural disorder dictates the thermal transport of the hybrid metalcone films. By manipulating disorder and hence sound speed, thermal conductivity of the polymer films can be changed. Specifically, we find that films with a higher degree of disorder have a lower thermal conductivity. We further verify our conclusion by measuring the volumetric heat capacity and vibrational lifetime of a disordered and an ordered alucone film. The thermal transport mechanisms depicted in this study can also be applied to organic and inorganic polymer films.

Acknowledgement

M.S.B.H, S.Z., and P.E.H. appreciate support from the Army Research Office, Grant Number W911NF-16-1-0406 and the National Science Foundation, Grant Number 2318576. R.A.N., S.A., S.W., and G.P. also acknowledge support from the Army Research Office, Grant Number W911NF-16-1-0406.

Supporting Information

S1. Metalcone deposition conditions

During metalcone deposition, purified nitrogen (N_2 , 99.999%, Arc3 Gases) is used as the carrier and purge gas. In the cylindrical reactor, tincone is deposited from TDMASn/EG following (10 s chamber evacuation/3 s TMDASn dose/60 s N_2 purge)/(0.3 s EG dose/60 s N_2 purge) and alucone is deposited from TMA/EG following (0.2 s TMA dose/60 s N_2 purge)/(0.2 s EG dose/60 s N_2 purge). In the spherical chamber, alucone is deposited from TMA/HDO following (0.4 s TMA dose/45 s N_2 purge)/(30 s chamber evacuation/8 s HDO dose/45 s N_2 purge).

S2. Metalcone film characterizations

Metalcone film thickness is measured with ellipsometry either in situ (Film Sense FS-1 multiwavelength ellipsometer) or ex situ (J. A. Woollam Co. alpha-SE spectroscopic ellipsometer) at an incidence angle of $\sim 70^\circ$ relative to the surface normal. In situ data is collected at 436, 521, 599, and 638 nm while ex situ data is collected from 300 to 900 nm. Thickness is determined from a Cauchy model available with each ellipsometer's software package. Uncertainty in film thickness is generally a few percent.

S3. Picosecond acoustics of disordered alucone films

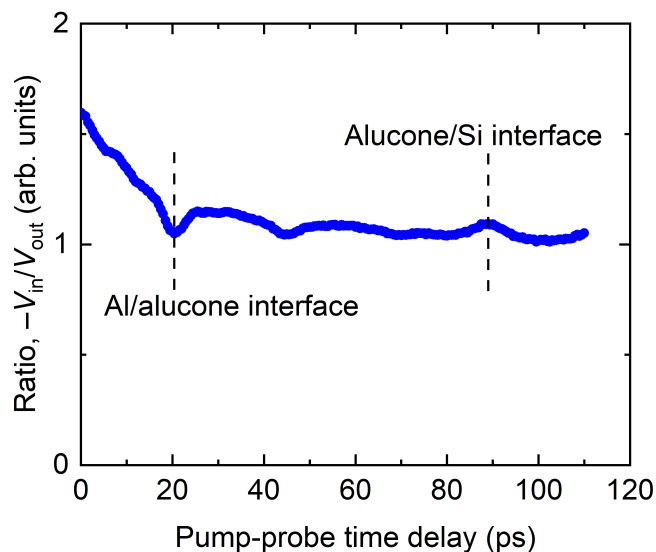


Figure S1: Picosecond acoustic response of the 156 nm disordered alucone film.

Table S1: Thermal conductivity and longitudinal sound speed of the polymers shown in Figure 2(d).

Polymers	Thermal conductivity (W m ⁻¹ K ⁻¹)	Longitudinal sound speed (m s ⁻¹)
PVA	0.31	3210 ⁷
PAA	0.37	3740 ⁷
PVP	0.27	3180 ⁷
PAM	0.38	4340 ⁷
PSS	0.38	3640 ⁷
MC	0.21	2770 ⁷
PMMA	0.20	2850 ⁷
PAP	0.16	2640 ⁷
PALi	0.55	5100 ²⁹
PANa	0.45	4100 ²⁹
PACa	0.49	4800 ²⁹
PAFe	0.51	5000 ²⁹
PACu	0.5	4800 ²⁹
PVPA	0.44	3900 ²⁹
PVPLi	0.63	5300 ²⁹
PVPMg	0.66	5400 ²⁹
PVPCa	0.67	5300 ²⁹
PVSNa	0.42	4300 ²⁹
PDDA	0.29	3700 ²⁹
PAH	0.34	4300 ²⁹
PMPC	0.21	3300 ²⁹
PS	0.141	2380 ²⁹
ADP	0.15	2850 ²⁹
DSQ	0.14	2100 ²⁹
Vectra	1.7	6879 ⁸
Kevlar	3.2	10203 ⁸
M5 AS	8.9	9772 ⁸
Spectra 900	11.5	10275 ⁸
Spectra 2000	16	12343 ⁸
Dyneema	14.2	11404 ⁸
PBT	12.7	13929 ⁸
Zylon AS	18.5	12187 ⁸
Zylon HM	23	14850 ⁸

Table S2: Gaussian oscillator parameters used to fit the ordered alucone film data, resulting in a mean square error of 1.36.

Oscillator No.	Amplitude	Centroid Frequency (cm^{-1})	Centroid Wavelength (μm)	Broadening (cm^{-1})	Lifetime (fs)
1	0.19	3439.7	2.91	310.0	17.13 ± 1.82
2	0.13	3110.1	3.22	606.6	8.75 ± 1.52
3	0.22	1607.6	6.22	127.2	41.75 ± 3.04
4	0.26	1441.1	6.94	201.0	26.42 ± 2.43
5	0.07	1224.6	8.17	26.7	198.81 ± 96.13
6	0.45	1030.8	9.70	253.8	20.92 ± 3.61
7	0.85	791.65	12.63	234.4	22.65 ± 7.93
8	2.12	667.83	14.97	99.6	53.31 ± 6.74

Table S3: Gaussian oscillator parameters used to fit the disordered Alucone film, resulting in a mean square error of 0.37.

Oscillator No.	Amplitude	Centroid Frequency (cm^{-1})	Centroid Wavelength (μm)	Broadening (cm^{-1})	Lifetime (fs)
1	0.11	3487.6	2.87	220.9	24.03 ± 7.32
2	0.15	3259.1	3.07	352.8	15.05 ± 11.41
3	0.08	2912.4	3.43	231.6	22.92 ± 5.57
4	0.04	2578.4	3.88	960.3	5.53 ± 1.73
5	0.23	1590.7	6.29	148.9	35.66 ± 1.38
6	0.21	1414.2	7.07	107.8	49.26 ± 2.83
7	0.07	1259.6	7.94	81.1	65.43 ± 12.79
8	0.36	995.6	10.04	303.6	17.48 ± 2.1
9	0.46	756.3	13.22	189.6	28.01 ± 14.41
10	1.04	667.8	14.98	100.2	52.99 ± 10.37

References

- [1] Duda, J. C.; Hopkins, P. E.; Shen, Y.; Gupta, M. C. Thermal transport in organic semiconducting polymers. *Applied Physics Letters* **2013**, *102*, 251912.
- [2] Chen, L.; Huang, Z.; Shahbazian-Yassar, R.; Libera, J. A.; Klavetter, K. C.; Zavadil, K. R.; Elam, J. W. Directly formed alucone on lithium metal for high-performance Li batteries and Li-S batteries with high sulfur mass loading. *ACS applied materials & interfaces* **2018**, *10*, 7043–7051.
- [3] DeCoster, M. E.; Meyer, K. E.; Piercy, B. D.; Gaskins, J. T.; Donovan, B. F.; Giri, A.; Strnad, N. A.; Potrepka, D. M.; Wilson, A. A.; Losego, M. D.; others Density and size effects on the thermal conductivity of atomic layer deposited TiO₂ and Al₂O₃ thin films. *Thin Solid Films* **2018**, *650*, 71–77.
- [4] Li, H.; DeCoster, M. E.; Ming, C.; Wang, M.; Chen, Y.; Hopkins, P. E.; Chen, L.; Katz, H. E. Enhanced molecular doping for high conductivity in polymers with volume freed for dopants. *Macromolecules* **2019**, *52*, 9804–9812.
- [5] Nye, R. A.; Kelliher, A. P.; Gaskins, J. T.; Hopkins, P. E.; Parsons, G. N. Understanding molecular layer deposition growth mechanisms in polyurea via picosecond acoustics analysis. *Chemistry of Materials* **2020**, *32*, 1553–1563.
- [6] Ma, H.; Lioni, K.; Magbitang, T. P.; Gaskins, J.; Hopkins, P. E.; Huxtable, S. T.; Tian, Z. Pore-Confined Polymers Enhance the Thermal Conductivity of Polymer Nanocomposites. *ACS Macro Letters* **2021**, *11*, 116–120.
- [7] Xie, X.; Li, D.; Tsai, T.-H.; Liu, J.; Braun, P. V.; Cahill, D. G. Thermal conductivity, heat capacity, and elastic constants of water-soluble polymers and polymer blends. *Macromolecules* **2016**, *49*, 972–978.
- [8] Wang, X.; Ho, V.; Segalman, R. A.; Cahill, D. G. Thermal conductivity of high-modulus polymer fibers. *Macromolecules* **2013**, *46*, 4937–4943.
- [9] Singh, V.; Bougher, T. L.; Weathers, A.; Cai, Y.; Bi, K.; Pettes, M. T.; McMenamin, S. A.; Lv, W.; Resler, D. P.; Gattuso, T. R.; others High thermal conductivity of chain-oriented amorphous polythiophene. *Nature nanotechnology* **2014**, *9*, 384–390.
- [10] Kim, G.-H.; Lee, D.; Shanker, A.; Shao, L.; Kwon, M. S.; Gidley, D.; Kim, J.; Pipe, K. P. High thermal conductivity in amorphous polymer blends by engineered interchain interactions. *Nature materials* **2015**, *14*, 295–300.
- [11] Xu, X.; Chen, J.; Zhou, J.; Li, B. Thermal conductivity of polymers and their nanocomposites. *Advanced Materials* **2018**, *30*, 1705544.
- [12] Lv, G.; Soman, B.; Shan, N.; Evans, C. M.; Cahill, D. G. Effect of linker length and temperature on the thermal conductivity of ethylene dynamic networks. *ACS Macro Letters* **2021**, *10*, 1088–1093.
- [13] Lv, G.; Jensen, E.; Shan, N.; Evans, C. M.; Cahill, D. G. Effect of aromatic/aliphatic structure and cross-linking density on the thermal conductivity of epoxy resins. *ACS Applied Polymer Materials* **2021**, *3*, 1555–1562.
- [14] Dameron, A.; Seghete, D.; Burton, B.; Davidson, S.; Cavanagh, A.; Bertrand, J.; George, S. Molecular layer deposition of alucone polymer films using trimethylaluminum and ethylene glycol. *Chemistry of Materials* **2008**, *20*, 3315–3326.

- [15] Zhao, Y.; Goncharova, L. V.; Zhang, Q.; Kaghazchi, P.; Sun, Q.; Lushington, A.; Wang, B.; Li, R.; Sun, X. Inorganic–organic coating via molecular layer deposition enables long life sodium metal anode. *Nano letters* **2017**, *17*, 5653–5659.
- [16] Kaliyappan, K.; Or, T.; Deng, Y.-P.; Hu, Y.; Bai, Z.; Chen, Z. Constructing safe and durable high-voltage P2 layered cathodes for sodium ion batteries enabled by molecular layer deposition of alucone. *Advanced Functional Materials* **2020**, *30*, 1910251.
- [17] Han, J.-H.; Kim, T.-Y.; Kim, D.-Y.; Yang, H. L.; Park, J.-S. Water vapor and hydrogen gas diffusion barrier characteristics of Al₂O₃–alucone multi-layer structures for flexible OLED display applications. *Dalton Transactions* **2021**, *50*, 15841–15848.
- [18] Braun, J. L.; Olson, D. H.; Gaskins, J. T.; Hopkins, P. E. A steady-state thermoreflectance method to measure thermal conductivity. *Review of Scientific Instruments* **2019**, *90*.
- [19] Hoque, M. S. B.; Koh, Y. R.; Aryana, K.; Hoglund, E. R.; Braun, J. L.; Olson, D. H.; Gaskins, J. T.; Ahmad, H.; Elahi, M. M. M.; Hite, J. K.; others Thermal conductivity measurements of sub-surface buried substrates by steady-state thermoreflectance. *Review of Scientific Instruments* **2021**, *92*.
- [20] Hoque, M. S. B.; Koh, Y. R.; Braun, J. L.; Mamun, A.; Liu, Z.; Huynh, K.; Liao, M. E.; Hussain, K.; Cheng, Z.; Hoglund, E. R.; others High in-plane thermal conductivity of aluminum nitride thin films. *ACS nano* **2021**, *15*, 9588–9599.
- [21] Cahill, D. G. Analysis of heat flow in layered structures for time-domain thermoreflectance. *Review of scientific instruments* **2004**, *75*, 5119–5122.
- [22] Feser, J. P.; Liu, J.; Cahill, D. G. Pump-probe measurements of the thermal conductivity tensor for materials lacking in-plane symmetry. *Review of Scientific Instruments* **2014**, *85*.
- [23] Jiang, P.; Qian, X.; Yang, R. Tutorial: Time-domain thermoreflectance (TDTR) for thermal property characterization of bulk and thin film materials. *Journal of Applied Physics* **2018**, *124*.
- [24] Peng, Q.; Gong, B.; VanGundy, R. M.; Parsons, G. N. “Zincone” zinc oxide- organic hybrid polymer thin films formed by molecular layer deposition. *Chemistry of Materials* **2009**, *21*, 820–830.
- [25] Nye, R. A.; Wang, S.; Uhlenbrock, S.; Smythe, J. A.; Parsons, G. N. In situ analysis of growth rate evolution during molecular layer deposition of ultra-thin polyurea films using aliphatic and aromatic precursors. *Dalton Transactions* **2022**, *51*, 1838–1849.
- [26] Bergsman, D. S.; Closser, R. G.; Tassone, C. J.; Clemens, B. M.; Nordlund, D.; Bent, S. F. Effect of backbone chemistry on the structure of polyurea films deposited by molecular layer deposition. *Chemistry of Materials* **2017**, *29*, 1192–1203.
- [27] George, S. M.; Lee, B. H.; Yoon, B.; Abdulagatov, A. I.; Hall, R. A. Metalcones: Hybrid organic–inorganic films fabricated using atomic and molecular layer deposition techniques. *Journal of Nanoscience and Nanotechnology* **2011**, *11*, 7948–7955.
- [28] Bergsman, D. S.; Closser, R. G.; Bent, S. F. Mechanistic studies of chain termination and monomer absorption in molecular layer deposition. *Chemistry of Materials* **2018**, *30*, 5087–5097.
- [29] Xie, X.; Yang, K.; Li, D.; Tsai, T.-H.; Shin, J.; Braun, P. V.; Cahill, D. G. High and low thermal conductivity of amorphous macromolecules. *Physical Review B* **2017**, *95*, 035406.

- [30] Hoque, M. S. B.; Brummel, I. A.; Høglund, E. R.; Dionne, C. J.; Aryana, K.; Tomko, J. A.; Gaskins, J. T.; Hirt, D.; Smith, S. W.; Beechem, T.; others Interface-independent sound speed and thermal conductivity of atomic-layer-deposition-grown amorphous AlN/Al₂O₃ multilayers with varying oxygen composition. *Physical Review Materials* **2023**, *7*, 025401.
- [31] DeCoster, M. E.; Chen, X.; Zhang, K.; Rost, C. M.; Høglund, E. R.; Howe, J. M.; Beechem, T. E.; Baumgart, H.; Hopkins, P. E. Thermal conductivity and phonon scattering processes of ALD grown PbTe–PbSe thermoelectric thin films. *Advanced Functional Materials* **2019**, *29*, 1904073.
- [32] Aryana, K.; Gaskins, J.; Nag, J.; Read, J.; Olson, D.; Grobis, M.; Hopkins, P. Thermal properties of carbon nitride toward use as an electrode in phase change memory devices. *Applied Physics Letters* **2020**, *116*.
- [33] Braun, J. L.; King, S. W.; Giri, A.; Gaskins, J. T.; Sato, M.; Fujiseki, T.; Fujiwara, H.; Hopkins, P. E. Breaking network connectivity leads to ultralow thermal conductivities in fully dense amorphous solids. *Applied Physics Letters* **2016**, *109*.
- [34] Braun, J. L.; Rost, C. M.; Lim, M.; Giri, A.; Olson, D. H.; Kotsonis, G. N.; Stan, G.; Brenner, D. W.; Maria, J.-P.; Hopkins, P. E. Charge-induced disorder controls the thermal conductivity of entropy-stabilized oxides. *Advanced materials* **2018**, *30*, 1805004.
- [35] Gorham, C. S.; Gaskins, J. T.; Parsons, G. N.; Losego, M. D.; Hopkins, P. E. Density dependence of the room temperature thermal conductivity of atomic layer deposition-grown amorphous alumina (Al₂O₃). *Applied Physics Letters* **2014**, *104*.
- [36] Aryana, K.; Gaskins, J. T.; Nag, J.; Stewart, D. A.; Bai, Z.; Mukhopadhyay, S.; Read, J. C.; Olson, D. H.; Høglund, E. R.; Howe, J. M.; others Interface controlled thermal resistances of ultra-thin chalcogenide-based phase change memory devices. *Nature Communications* **2021**, *12*, 774.
- [37] Shankar, A. N.; Netravali, A. N.; Mensah, R. A.; Das, O. Microscale combustion calorimetry assessment of green composites made with chicken feather-modified soy protein resins and jute fabric. *Composites Part C: Open Access* **2023**, *12*, 100394.
- [38] Olson, D. H.; Rost, C. M.; Gaskins, J. T.; Szwejkowski, C. J.; Braun, J. L.; Hopkins, P. E. Size effects on the cross-plane thermal conductivity of transparent conducting indium tin oxide and fluorine tin oxide thin films. *IEEE Transactions on Components, Packaging and Manufacturing Technology* **2018**, *9*, 51–57.
- [39] Aryana, K.; Zhang, Y.; Tomko, J. A.; Hoque, M. S. B.; Høglund, E. R.; Olson, D. H.; Nag, J.; Read, J. C.; Ríos, C.; Hu, J.; others Suppressed electronic contribution in thermal conductivity of Ge₂Sb₂Se₄Te. *Nature Communications* **2021**, *12*, 7187.